HOKKAIDO UNIVERSITY

Title	Recrystallization Texture of Cold-rolled Oxide Dispersion Strengthened Ferritic Steel
Author(s)	Leng, Bin; Ukai, Shigeharu; Sugino, Yoshito et al.
Citation	ISIJ International, 51(6), 951-957 https://doi.org/10.2355/isijinternational.51.951
Issue Date	2011-06-15
Doc URL	https://hdl.handle.net/2115/76320
Rights	著作権は日本鉄鋼協会にある
Type	journal article
File Information	ISIJ Int. 51(6)_ 951-957 (2011).pdf

Hokkaido University Collection of Scholarly and Academic Papers : HUSCAP

ISIJ International, Vol. 51 (2011), No. 6, pp. 951–957

Recrystallization Texture of Cold-rolled Oxide Dispersion Strengthened Ferritic Steel

Bin LENG,[1)] Shigeharu UKAI,[1)] Yoshito SUGINO,[1)] Qingxin TANG,[1)] Takeshi NARITA,[1)] Shigenari HAYASHI,[1)] Farong WAN,[2)] Satoshi OHTSUKA[3)] and Takeji KAITO[3)]

1) Faculty of Engineering, Hokkaido University. E-mail: bin.leng@yahoo.com, s-ukai@eng.hokudai.ac.jp, y-sugino@eng.hokudai.ac.jp, tang.hokudai@gmail.com, tanari3@mmc.co.jp, hayashi@eng.hokudai.ac.jp 2) School of Materials Science and Engineering, University of Science and Technology Beijing. E-mail: wanfr@mater.ustb.edu.cn
3) Japan Atomic Energy Agency. E-mail: ohtsuka.satoshi@jaea.go.jp, kaito.takeji@jaea.gp.jp

(*Received on January 4, 2011; accepted on March 7, 2011*)

The recrystallization behavior of a 88% cold-rolled 15Cr–ODS ferritic steel was investigated. Specimens annealed at low and high temperatures show two different recrystallization modes. Annealing at 1 000°C generates a structure consisting of coarse grains with {110}<112> texture, while annealing at 1 150°C and 1 300°C produce fine grains with {111}<112> texture. This phenomenon is ascribed to that the mobility of boundaries between {110}<112> nuclei and {001}<110> deformed matrix are higher than between {111}<112> nuclei and {001}<110> deformed matrix. Also it is found that a recovery annealing at 900°C prior to recrystallization annealing will retard recrystallization, which results in a structure of coarse grains with {110}<112> texture even after the following annealing at 1 300°C.

KEY WORDS: ODS ferritic steel; cold-rolling; recrystallization; texture.

1. Introduction

Oxide-dispersion-strengthened (ODS) ferritic steels have excellent radiation resistance and better creep strength, which make them promising candidates for cladding tubes in advanced fast reactors.[1–3)] During the manufacturing process of ODS cladding tubes, the alloys undergo a series of cold-rolling and intermediate annealing,[4,5)] during which the microstructure of alloys are severely affected and different types of texture are produced. Analyses of the changes of microstructure and texture during cold-rolling and the following annealing are essential for optimizing the fabrication procedure in order to obtain the materials with high performances.

Because of the tremendous industrial importance, many authors have studied the recrystallization behaviors of ferritic steels, such as interstitial free (IF) steel[6–8)] and silicon steel.[9–12)] Nevertheless, fewer works of recrystallization texture of cold-rolled ODS ferritic steels have been reported.[13–16)] Therefore, this work focuses on the texture change during cold-rolling and the following annealing in 15Cr–ODS ferritic steels.

2. Experimental Procedure

The alloy with a composition of Fe–15Cr–0.03C–2W–$0.3Y_2O_3$ (mass%) was produced by mechanical alloying a mixture of metal and yttria powders using high energy ball mill. The resultant powder was subsequently consolidated by hot extrusion and forging at 1 150°C to make a 25 mm diameter bar. The steel bar was then annealed at 1 150°C for 1 h. A plate with size of 11 mm × 15 mm × 20 mm was cut from the center of the bar for cold-rolling. The rolling reduction was 88% and the rolling direction was parallel to the extrusion direction. After cold-rolling, the as cold-rolled plate was cut into small specimens for the isothermal annealing experiment at different temperatures in air. A JOEL JSM-6500 FE-SEM with EBSD system was used to observe the microstructure and texture of specimens, and the data processing was done with the help of TSL OIM Analysis 4.5 software.

3. Results

3.1. Before Cold-rolling

Before cold-rolling, though the alloy was extruded and forged at 1 150°C and followed by an annealing at the same temperature for 1 hr, it still had a structure of deformed state with elongated fine grains about 2 μm in average size (**Fig. 1**(a)). And these fine grains are not subgrains, but real grains with high angle boundaries (Boundaries with misorientations larger than 15° were marked by black line in Fig. 1(a)). And such refinement of grain size is due to the extensively dispersion of nano-sized oxide particles.

From the φ_2=45° section of ODF (Fig. 1(b)), we can see that the specimen before cold-rolling has a strong <110>// RD α-fibre texture. And the numbers on ODF represent the texture intensity, for example in Fig. 1(b), max=9.22 means that the most preferential orientation has the intensity 9.22 times as random distribution intensity. These are consist with the works on extruded ODS steels reported before.[17)]

© 2011 ISIJ

3.2. As-cold-rolled State

After the cold-rolling with a high reduction of 88%, morphology of grains on the rolling plane almost does not change, still fine and elongated (**Fig. 2**(a)). However, their texture are different. The φ_2=45° section of ODF (Fig. 2(b)) shows that the as-cold-rolled texture contains both α-fibre such as {001}<110>, {112}<110> and γ-fibre like {111}<110> and {111}<112>. Among all the texture components, {001}<110> has the highest intensity of approximately 18 times random.

3.3. Annealing at 1 000°C

The as-cold-rolled specimens were annealed at 1 000°C for different durations. In order to avoid the influence on recrystallization behavior caused by differences in the initial strain condition, the same specimen was annealed and

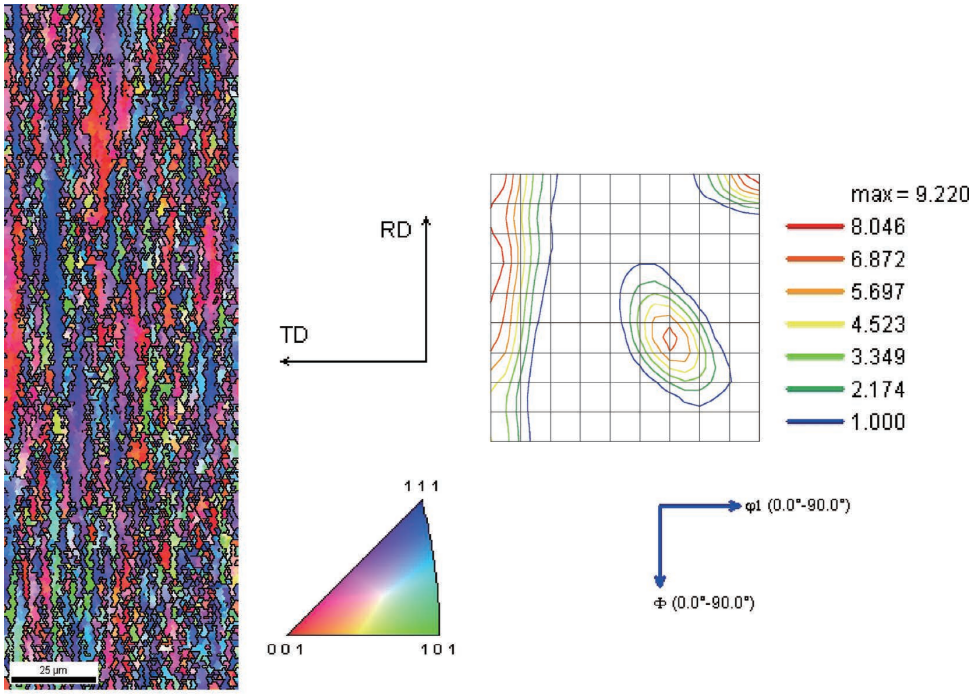

Fig. 1. Results of texture analyses before cold-rolling: (a) Inverse pole figure (IPF), (b) $\varphi 2$ =45° section of ODF (Orientation distribution function).

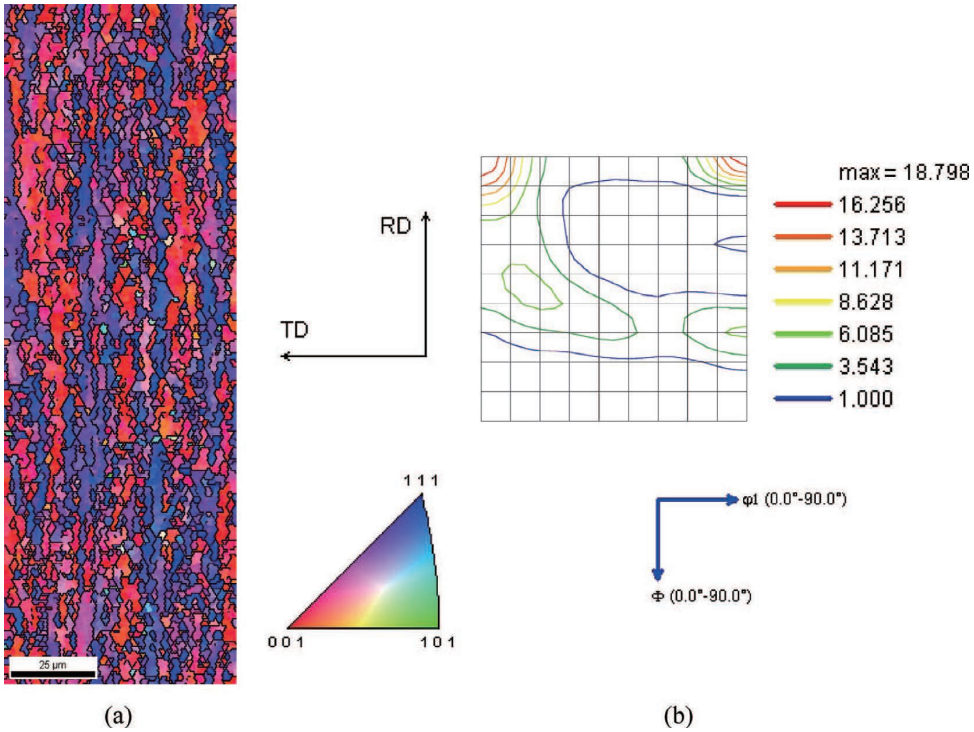

Fig. 2. Results of texture analyses after cold-rolling: (a) IPF of as-cold-rolled specimen, (b) $\varphi 2$ =45° section of ODF.

© 2011 ISIJ

observed four times with different annealing durations; at each observation, EBSD mappings covered the whole area of the specimen's surface. **Figure 3** shows that the process of recrystallization was very slow when specimen was annealed at 1 000°C, finished after more than 5 hrs. The recrystallized specimens contain very large and elongated grains which are about several hundred micron in size, and most of these grains have orientations close to {110}<112>, showing a sharp texture (Fig. 3(e)).

3.4. Annealing at 1 150°C and 1 300°C

After increasing the annealing temperature, it is found that the recrystallization mode changes as it is showed in **Fig. 4**: First, the recrystallization rate become faster, specimens annealed at both 1 150°C and 1 300°C for 5 mins are completely recrystallized, and their final grain size are smaller comparing with the 1 000°C annealed specimen. Second, the recrystallization texture change to {111}<112> instead of {110}<112>. From Figs. 4(a), 4(c), we can see that although most grains have the orientations of {111}<112> (colored in blue on IPF), there are still a number of grains have {110}<112> orientation (colored in green on IPF) and their sizes are bigger than the sizes of those with {111}<112> orientation.

3.5. Two-step Annealing

The above experiments are one-step annealing of cold-rolled specimens at a temperature higher than recrystallization temperature. However, during the manufacturing process of cladding tubes, the tubes usually undergo several intermediate annealing without recrystallization in order to reduce hardness for next cold-rolling. A two-step annealing experiment was, therefore, designed to determine the effect of recovery on the following recrystallization. The specimen was first annealed at 900°C for 2 hrs, and it was shown that the recovered specimen had the same microstructure as as-cold rolled state (**Figs. 5**(a), 5(b)). Then this specimen was again annealed at 1 000°C, which is the recrystallization temperature, for 24 hrs but didn't recrystallized (Figs. 5(c), 5(d)). Again, increasing the annealing temperature to 1 300°C for 1 hr, the recrystallized structure of coarse {110}<112> grains (Figs. 5(e), 5(f)), which used to happen at 1 000°C during one-step annealing, was obtained. It seemed that recrystallization is retarded due to the recovery annealing before final annealing.

4. Discussion

The experimental results show that in the recrystallized ODS ferritic steel, most of the grains have the orientation of {110}<112> or {111}<112>. {110}<112> is not a common texture component in BCC materials and it rotates 35.3° with [110] axis from the well known {110}<001> Goss orientation; {111}<112> ,which belongs to γ-fibre, is usually found in both deformed and recrystallized ferritic steels.[18] The proportions of these two recrystallized texture components are different depending on annealing temperature. When annealed at low temperature, {110}<112> dominates while annealed at high temperature {111}<112> dominates.

Since the orientation of nucleus is present in the deformed structure,[18] we can infer that there are both {110}<112> and {111}<112> nuclei already exist in the cold-rolled or recovered states. However, the process how these nuclei formed and their exact content in the deformed state is not clear now. From the ODF of the deformed state (Figs. 2(b), 5(b), 5(d)), no clue of the existence of {110}<112> nuclei could be found, which may ascribed to either their small quantity or their small size. And despite that there is a certain content of {111}<112> in ODF, it is difficult to regard it as {111}<112> nucleus since it is also one of the typical texture components of cold-rolled BCC metals.

To make a compromise, we neglect the period of nucleation, considering the recrystallization process as the growth of pre-exist nuclei at the expense of surrounding deformed matrix to release stored energy. The growth rate is expressed as $V=M \times F$, where M is boundary mobility between the nucleus and the surrounding deformed matrix, F is the driving force of recrystallization. $F=Ed-P$, where Ed is the stored energy of deformed matrix and P is the pinning force of dispersed oxide particles. Because of the homogeneous dispersion of oxide particles in this material, the pinning force P is considered to be constant for both {110}<112> and {111}<112> nuclei. The stored energy Ed depends on the orientation of the deformed matrix. Based on the published data,[19,20] we know that $Ed_{\{111\}} > Ed_{\{112\}} > Ed_{\{001\}}$. Therefore, driving force $F_{\{001\}}$ is lowest when a nucleus tries to grow into {001}<110> deformed matrix. Besides, noticing that {001}<110> has the highest intensity among all the deformed components (Fig. 2(b)), we could infer that the abundant existence of this low stored energy deformed matrix has a great impact on the overall growth rate. However, to make sure whether overall growth rate is determined by the growth rate of nuclei overcome {001}<110> deformed matrix, we also need to take boundary mobility into consideration.

Boundary mobility $M=M_0\exp(-Q/RT)$ is sensitive to both temperature and boundary characteristic. There are several theories that have explained how a certain kind of grain boundary possesses advantage in mobility and subsequently results in a recrystallization texture: T. Urabe[6] and L. Kestens[8] proposed a selective growth theory in which nuclei possessing favorable <110> axis rotation relationships with respect to the deformed matrix undergo preferential growth. J. Harase[9] and Y. Ushigami[10] claimed that coincidence site lattice (CSL) boundary plays a key role in developing Goss texture during secondary recrystallization of Fe–3%Si alloy. Y. Hayakawa's research on electrical Fe–Si steels[11,12] reveals that grain boundaries which have misorientation of 20–45° have highest energies and have higher mobility than low energy boundaries.

Table 1 shows the misorientation of boundaries between nuclei and the surrounding deformed matrix, for example 46°@[2,-24,-5] means there is a boundary with misorientation of 46° with [2,-24,-5] rotation axis between {110}<112> nucleus and {001}<110> deformed matrix. From Table 1 we can see that most of the rotation axes are random axis and the CSL boundaries are absent. Therefore, high energy boundary theory seems to be more suitable in our case than rotation axis theory and CSL boundary theory. It is clear that the boundaries between two kinds of nuclei and {112}<110>, {111}<110> matrix have similar misorientation of 30° and 35.6°, which are recognized as high

© 2011 ISIJ

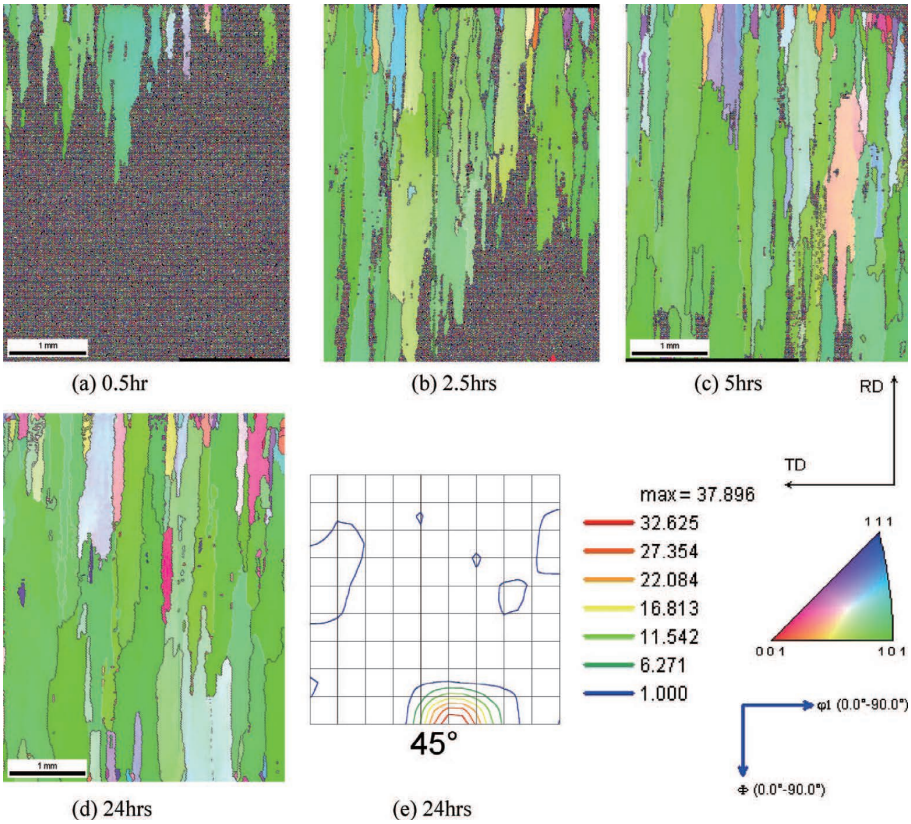

Fig. 3. Inverse pole figure of specimen annealed at 1 000°C for (a) 0.5 hr, (b) 2.5 hrs, (c) 5 hrs, (d) 24 hrs and (e) $\varphi 2$ =45° section of ODF of specimen annealed at 1 000°C for 24 hrs.

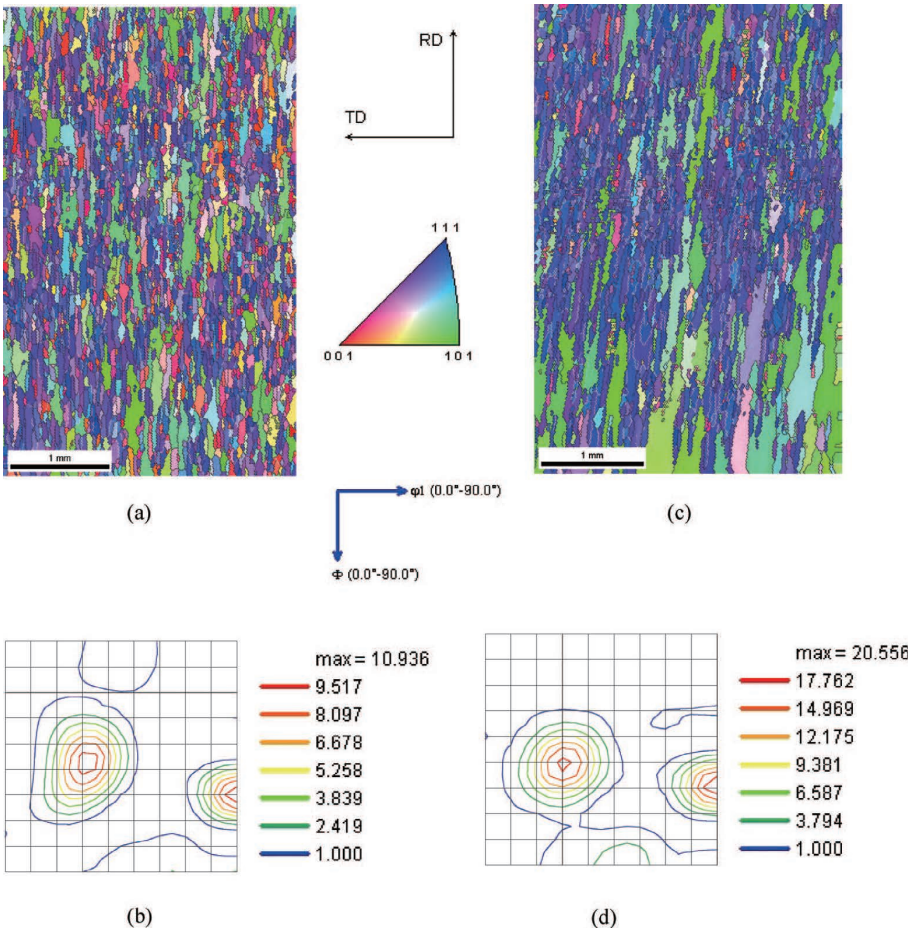

Fig. 4. Specimen annealed at 1 150°C for 5 mins: (a) IPF, (b) $\varphi 2$ =45° section of ODF and annealed at 1 300°C for 5 mins: (c) IPF, (d) $\varphi 2$ =45° section of ODF.

© 2011 ISIJ

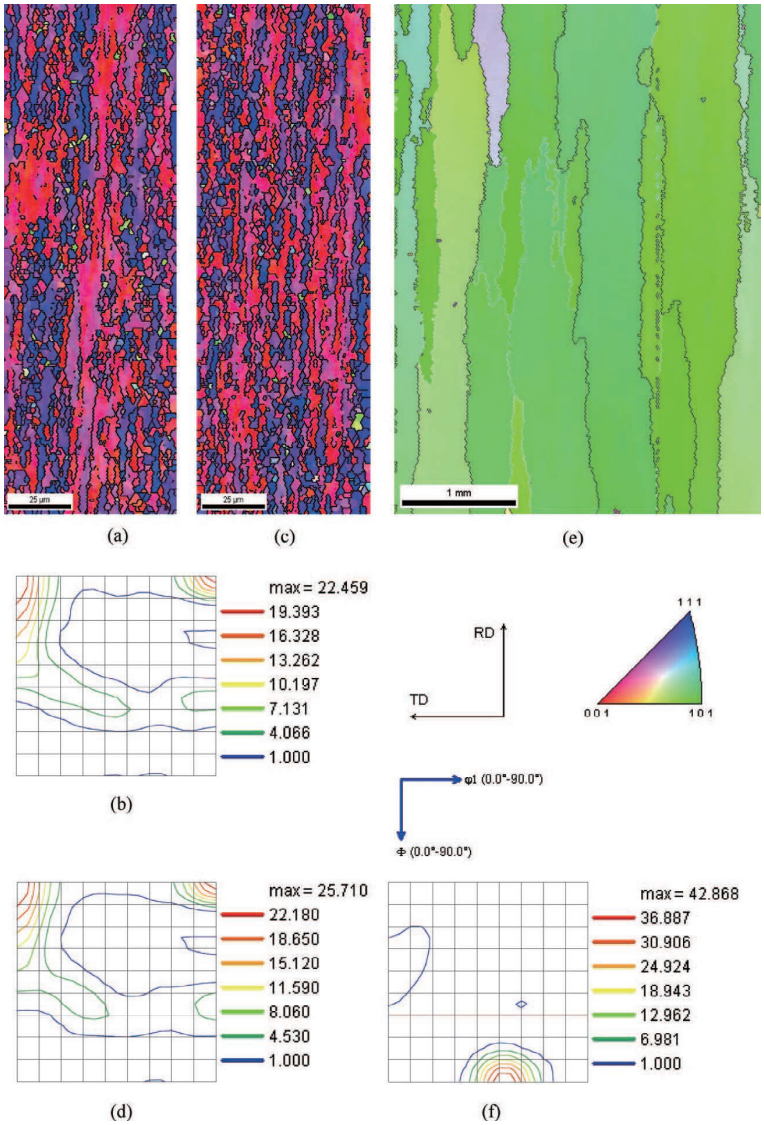

Fig. 5. Specimen underwent two step annealing, first recovery annealed at 900°C for 2 hrs: (a) IPF, (b) ODF then recrystallization annealed at 1 000°C for 24 hrs: (c) IPF, (d) $\varphi 2$=45° section of ODF and 1 300°C for 1 hr: (e) IPF, (f) $\varphi 2$=45° section of ODF.

Table 1. Misorientation of boundaries between deformed matrix and nuclei.

deformed matrix / nucleus	{001}<110>	{112}<110>	{111}<110>	{111}<112>
{110}<112>	46°@[2,-24,-5]	30°@[1,1,-1]	35.6°@[16,1,-12]	42.8°@[2,-2,11]
{111}<112>	54.7°@[110]	35.6°@[1,16,12]	30°@[1,1,1]	0°

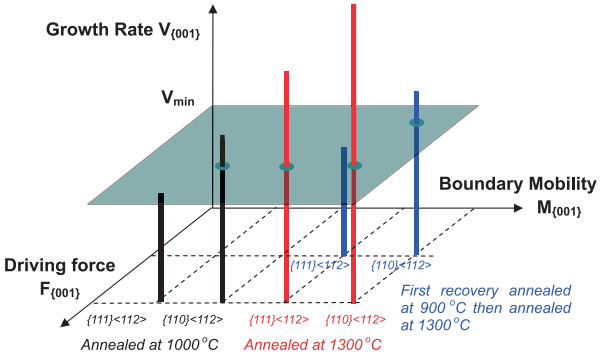

Fig. 6. Schematic of growth rate of two kinds of nuclei overcome {001}<110> under different heat-treatment conditions.

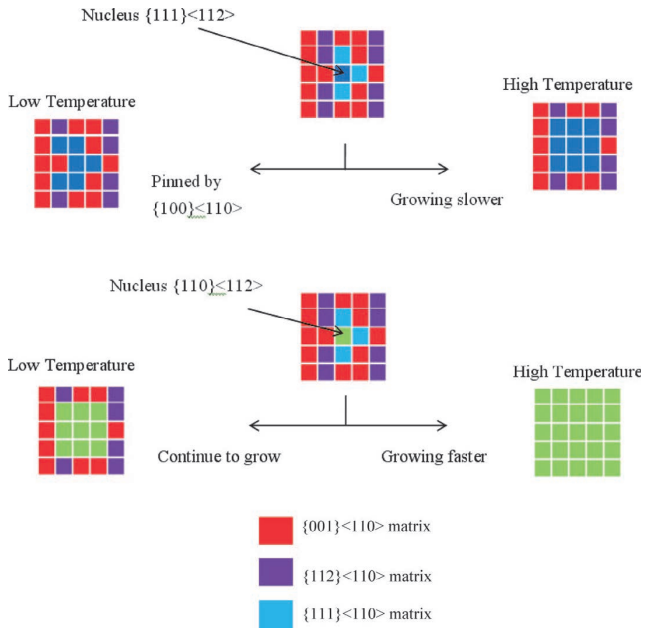

Fig. 7. Schematic view of nuclei growth at low and high temperature.

© 2011 ISIJ

mobility boundary according to Hayakawa's research. Though having a misorientation of 46°, we still regard boundaries between {110}<112> nuclei and {001}<110> matrix as high mobility boundaries, considering the deviation from ideal orientation in the practical steel. On the other hand, boundaries between {111}<112> nuclei and {001}<110> matrix will have lower mobility due to its 54.7° misorientation. The exact growth rate of boundaries in Table 1 are not clear, but if we roughly assume that all high mobility boundaries have the same mobility, we can say that the overall growth rate is limited by the rate of nuclei growing overcome {001}<110> deformed matrix, which has the lowest driving force for recrystallzation and has the highest texture intensity among all the deformed matrix. Thus, the mobility advantage of boundaries between {110}<112> nuclei and {001}<110> matrix over its counter part of {111}<112> nuclei, plays a key role in developing the final recrystallisation texture. Besides, it's difficult for {111}<112> nuclei to grow overcome {111}<112> deformed matrix because of the lacking of orientation gradient, which may also contribute to the overall growth rate advantage of {110}<112> nuclei, though not much due to the low content of this deformed component in the deformed state.

Since the overall growth rate is decided by the rate of nuclei growing overcome {001}<110> deformed matrix, we discuss the growth rate of two kinds of nuclei, {110}<112> and {111}<112>, overcome {001}<110> deformed matrix instead of the overall growth rate. **Figure 6** is a schematic showing how the driving force $F_{\{001\}}$ for a nucleus to grow overcome {001}<110> deformed matrix as well as boundary mobility $M_{\{001\}}$ between a nucleus and {001}<110> deformed matrix affect the recrystallization modes. Assuming that there is a minimum growth rate V_{min} for us to observe, and any nucleus with growth rate lower than V_{min} is considered to be pinned by {001}<110> matrix. Then we can see from Fig. 6: when annealed at 1 000°C, only {110}<112> nuclei can grow due to mobility advantage while {111}<112> nuclei are pinned by {001}<110> matrix. Therefore, the recrystallized material will have a texture almost full of {110}<112> component. Since there could be only a few {110}<112> nuclei exist in the cold-rolled matrix, the final grain size after recrystallization is very large. When annealed at higher temperature such as 1 300°C, the mobility of all boundaries become higher that even {111}<112> nuclei have enough growth rate to overcome {001}<100> deformed matrix. The mobility of {110}<112> nuclei are still higher than that of {111}<112> nuclei, which makes the final the size of {110}<112> grains larger than the size of {111}<112> grains. However, the strong {111}<112> texture after annealing at this temperature may be due to the existence of large amount of {111}<112> nuclei in deformed matrix, although we have no reasonable explanation for the frequency advantage of {111}<112> nuclei at present. This situation is schematically shown in **Fig. 7**. Now considering the situation of two-step annealing, during recovery annealing, part of the stored energy is released, thereby growth rate of both kinds of nuclei decrease due to lower of driving force. Even that the following annealing is executed at 1 300°C, only {110}<112> nuclei have the enough growth rate to overcome {001}<110> deformed matrix, resulting in a same texture as one-step annealing at 1 000°C.

At last, we attempt to investigate why {110}<112> can not become dominance in non-ODS ferritic steels using the theory above: After similar cold-rolling reduction, the intensity of {001}<110> texture, which suppress the growth of nuclei, in conventional ferritic steels[6,7] is lower comparing with our ODS steel. The possible reason of this difference is that the initial texture in ODS ferritic steel is hot-extrusion texture, while the initial texture of conventional ferritic steels which is hot band texture. Besides, oxide particles, which usually hinder the recrystallization by pinning grain boundaries, are absent in the conventional steels. Therefore, it is easier for nuclei to grow in conventional ferritic steels and the recrystallization temperature is lower, around 700°C.[6,7] From **Fig. 8**, we can see that the boundary mobility advantage of {110}<112>, ΔM, decreases with the decreasing of temperature. Consequently, in conventional ferritic steels, {110}<112> texture can not become dominance due to the diminishing of its boundary mobility advantage.

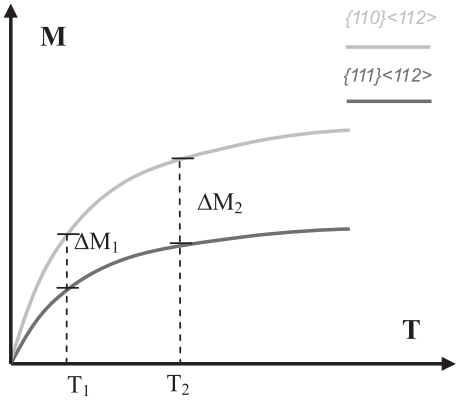

Fig. 8. Schematic of boundary mobility of nuclei overcome {001}<110> deformed matrix.

5. Conclusions

We investigated the recrystallization texture of 15Cr–ODS ferritic steel, and the following results were obtained.

(1) For 88% cold-rolled 15Cr–ODS ferritic steel, annealing at 1 000°C produces a strong {110}<112> texture and coarse grains while annealing at 1 150°C and 1 300°C produces a strong {111}<112> texture and relatively fine grains, this is an unique behavior of ODS ferritic steel.

(2) Low temperature recovery annealing at 900°C before recrystallization annealing will retard recrystallization, which results in a structure of coarse grains with {110}<112> texture even after the following final annealing at 1 300°C.

(3) These unique recrystalliztion texture formations are ascribed to the high amount of {001}<110> deformed grains in the cold-worked material, whose low stored energy make it the bottleneck for nuclei to grow. Its misorientation difference with the two recrystallization texture components, {111}<112> and {110}<112>, make a significant difference in boundary mobility, consequently affect the final recrystallization texture formation.

© 2011 ISIJ

REFERENCES

1) J. J. Huet, L. Coheur, A. De Bremaecker, L. De Wilde, J. Gedopt, W. Hendrix and W. Vandermeulen: *Nucl. Technol.*, **70** (1985), 215.
2) E. A. Little: Proc. of 17th Int. Symp. on Effects of Radiation on Materials, ASTM , Pennsylvania, (1996), 739.
3) S. Ukai, T. Nishida, T. Okuda and T. Yoshitake: *J. Nucl. Mater.*, **258–263** (1998), 1745.
4) S. Ukai, S. Mizuta, T. Yoshitake, T. Okuda, S. Hagi, M. Fujiwara and T. Kobayashi: *J. Nucl. Mater.*, **283–287** (2000), 702.
5) T. Narita, S. Ukai, T. Kaito, S. Ohtsuka and T. Kobayashi: *Nucl. Sci. Technol.*, **41** (2004), 1008.
6) T. Urabe and J. J. Jonas: *ISIJ Int.*, **34** (1994), 435.
7) J. L. Bocos, E. Novillo, M. M. Petite, A. Iza-Mendia and I. Gutierrez: *Metall. Mater. Trans.*, **34A** (2003), 827.
8) L. Kestens and J. J. Jonas: *Metall. Mater. Trans.*, **27A** (1996), 155.
9) J. Harase and R. Shimizu: *Trans. JIM*, **29** (1988), 388.
10) Y. Ushigami: *ISIJ Int.*, **38** (1998), 553.
11) Y. Hayakawa and J. A. Szpunar: *Acta Mater.*, **45** (1997), 1285.
12) Y. Hayakawa and J. A. Szpunar: *Acta Mater.*, **45** (1997), 4713.
13) T. S. Chou and H. K. D. H. Bhadeshia: *Metall. Trans. A.*, **24A** (1993), 773.
14) C. Capdevila, Y. L. Chen, N. C. K. Lassen, H. K. D. H. Bhadeshia and A. R. Jones: *Mater. Sci. Technol.*, **17** (2001), 693.
15) H. Regle and A. Alamo: *J. de Phys. IV. C7.*, **3** (1993), 727.
16) H. Okada, S. Ukai and M. Inoue: *J. Nucl. Sci. Technol.*, **33** (1996), 936.
17) E. A. Little, D. J. Mazey and W. Hanks: *Scr. Metall. Mater.*, **25** (1991), 1115.
18) F. J. Humphreys and M. Hatherly: Recrystallization and related annealing phenomena 2nd edition, Elsevier Press, Oxford, (2004), 258.
19) I. L. Dillamore and H. Katoh: *Met. Sci.*, **8** (1974), 73.
20) R. L. Every and M. Hatherly: *Texture*, **1** (1974), 183.

© 2011 ISIJ